Contents lists available at ScienceDirect

Electrochimica Acta

journal homepage: www.elsevier.com

Synthesis of polymer nanogels by electro-Fenton process: investigation of the effect of main operation parameters

Sonia Lanzalaco[a], Ignasi Sirés[b, *, 1], Maria Antonietta Sabatino[a], Clelia Dispenza[a], Onofrio Scialdone[a, 1], Alessandro Galia[a, *, 1]

[a] *Dipartimento dell'Innovazione Industriale e Digitale (DIID), Ingegneria Chimica, Gestionale, Informatica, Meccanica, Università degli Studi di Palermo, Viale delle Scienze, 90128 Palermo, Italy*

[b] *Laboratori d'Electroquímica dels Materials i del Medi Ambient, Departament de Química Física, Facultat de Química, Universitat de Barcelona, Martí i Franquès 1-11, 08028 Barcelona, Spain*

ARTICLE INFO

Article history:
Received 16 February 2017
Received in revised form 6 June 2017
Accepted 16 June 2017
Available online xxx

Keywords:
Electrochemical synthesis
Electro-Fenton process
Gas-diffusion electrode
Hydroxyl radical
Polymer crosslinking

ABSTRACT

Recently, electro-Fenton (EF) process has been shown as a promising, facile, effective, low cost and environmentally-friendly alternative for synthesizing polymer nanogels suitable as biocompatible nanocarriers for emerging biomedical applications. Here, the electrochemically-assisted modification of poly(vinylpyrrolidone) (PVP) by EF process was studied to assess the role of key operation parameters for a precise modulation of polymer crosslinking and its functionalization with —COOH and succinimide groups. The dimensions of the nanogels, in terms of hydrodynamic radius (R_h) and weight-average molecular weight (M_w), can be tuned up by controlling the electrolysis time, current density (j) and PVP and Fe^{2+} concentrations, as demonstrated via dynamic and static light scattering and gel permeation chromatography analysis. Using PVP at 0.25 wt.%, Fe^{2+} at 0.5-1.0 mmol dm^{-3} and low j, short treatment times induced intramolecular crosslinking with chain scission, allowing size reduction of PVP particles from 24 to 9–10 nm. Longer reaction times and higher PVP and Fe^{2+} contents favored intermolecular crosslinking ending in M_w values higher than the initial 3.95×10^5 g mol^{-1}. An excessive $^{\bullet}OH$ dose from a too high circulated charge (Q), i.e., too prolonged electrolysis time even at low j or too high j even for short time, promoted intramolecular crosslinking ($R_h \sim 10$–12 nm) along with a very significant chain scission probably owing to the loss of mobility of the three-dimensional nanogel network. In conclusion, EF allowed transforming the architecture of linear, inert PVP chains into a functionalized nanogel with —COOH and succinimide groups that have great potential for further conjugation.

1. Introduction

Nanogels are crosslinked polymer particles of nanoscale size (typically < 200 nm), which can be considered similar to hydrogels when they are composed of hydrophilic polymer chains [1,2]. Since the first appearance of this family of nanoscale materials, their application as biocompatible carriers for a large plethora of biomedical and biotechnological applications has been explored [3–5]. In particular, these soft materials have gained growing interest for drug delivery because of their high loading capacity and stability [6–10], showing also potential use as pH and temperature sensors [11,12]. They are also employed as in vivo imaging tracers [13], in water treatment [14] and catalysis [15], as smart gating membranes for the fabrication of active photonic crystals and coatings, and for generating bioactive scaffolds in regenerative medicine [16].

The classical method for nanogels manufacture is chemical crosslinking [17,18]. It involves the formation of covalent bonds between the polymer chains during polymerization of monomers with di- or multifunctional co-monomers (crosslinkers), or self-assembly processes that exploit various interactions of a preformed polymer [19]. Conventional and novel polymerization techniques allow the preparation of nanogels with different architectures including core–shell and hollow nanogel particles. Click chemistry, amide crosslinking, and photo-induced crosslinking are suitable synthetic approaches starting from polymer precursors [20], although an accurate control of the experimental parameters is crucial for fine tuning of final particle dimensions. In general, particle size must be limited to tens or few hundred nanometers, with a narrow particle size distribution [19].

A more recent synthesis approach makes recourse to pulse radiolysis of semi-dilute polymer aqueous solutions, relying on a high energy input to yield free hydroxyl radicals homogenously in the solution bulk from water lysis, which in turn allow the formation of radi-

* Corresponding authors.
Email addresses: sonia.lanzalaco@unipa.it (S. Lanzalaco); i.sires@ub.edu, isiresa@gmail.com (I. Sirés); mariaantonietta.sabatino@unipa.it (M.A. Sabatino); clelia.dispenza@unipa.it (C. Dispenza); onofrio.scialdone@unipa.it (O. Scialdone); alessandro.galia@unipa.it (A. Galia)
[1] Active ISE member.

http://dx.doi.org/10.1016/j.electacta.2017.06.097
0013-4686/

cals onto the preformed polymer chains via H-abstraction [21]. The intra/intermolecular recombination of active centers fosters polymer crosslinking. This is then a fast, clean route to prepare high purity nanogels with controlled particle size. [19,22,23]. Effective crosslinking of poly(vinylpyrrolidone) (PVP) [22–26], PVP copolymers [9,27,28] and other polymers [29] has been reported. As a major inconvenient, high energy radiation processes are not easily implementable into existing production lines, which limits their large-scale applicability.

Lately, the performance of alternative •OH-based methods requiring much simpler setups has been investigated. For example, the crosslinking of various preformed polymers like PVP and polyethyleneimine in water has been carried out by H_2O and H_2O_2 photolysis using UVC radiation [30,31]. In order to avoid the need of the expensive UVC lamps, some authors have performed crosslinking via chemical Fenton [32] and photo-Fenton [33] processes, whose efficacy is based on the occurrence of Fenton's reaction between added H_2O_2 and Fe^{2+} at optimal pH 2.8:

$$H_2O_2 + Fe^{2+} \rightarrow Fe^{3+} + {}^{\bullet}OH + OH^- \quad (1)$$

Fenton's approach is a hot topic nowadays, as demonstrated by its large impact in multiple domains. Its largest field of application is environmental chemistry, due to the great ability of •OH to inactivate microorganisms and degrade organic contaminants in water [34,35]. Fenton-based •OH has also been used to activate methane bond scission to form methanol for energy conversion [36]. In medicine, Fenton's free radicals trigger the lipid peroxidation, with a negative impact in cells and organs, being also detrimental for the digestion of proteins [37,38]. Conversely, •OH can act as a therapeutic agent to remove malignant tumors [39]. Regarding the synthesis of new materials, Fenton's reaction has been useful to apply Zn-doped carbon dots as biosensors with enhanced fluorescence [40] as well as to accelerate the crystallization of hydrothermal zeolite [41].

Worth mentioning, in addition to •OH (E^0 ($^{\bullet}OH/H_2O$) = 2.80 V|SHE) other radicals like $HO_2^{\bullet}$ (E^0 ($HO_2^{\bullet}/H_2O$) = 1.65 V|SHE) and $O_2^{\bullet -}$ (E^0 ($O_2^{\bullet -}/H_2O_2$) = 0.91 V|SHE) [29,37] formed in concomitant reactions due to the presence of the Fe^{3+}/Fe^{2+} couple, organic matter (R, R•) and, potentially, O_2, may have a role in the process. A very remarkable feature of Fenton and photo-Fenton processes is the occurrence of Fe^{2+} regeneration upon reduction of Fe^{3+} via chemical reaction with $HO_2^{\bullet}$, R• and/or $O_2^{\bullet -}$, thus being constant the production of •OH. However, the need of high concentrations of Fe^{2+} salts (up to 10 mmol dm^{-3}) constitutes a major drawback due to the complex product purification necessary to reduce the residual concentration to the low values required by biomedical specifications.

In this context, the electrochemical technology may expand the applicability of classical Fenton systems. The electro-Fenton (EF) process is one of the most widespread electrochemical advanced oxidation processes (EAOPs), especially in the field of water treatment [42,43]. In EF, the electrolytic cell is composed by a low or high oxidation power anode connected to a carbonaceous air-diffusion cathode with large ability to generate H_2O_2 on site as follows:

$$O_{2(g)} + 2\,H^+ + 2\,e^- \rightarrow H_2O_2 \quad (2)$$

Such in situ production is a very positive feature compared to classical Fenton, since it avoids the costs and risks from H_2O_2 production, transportation, handling and storage. Note that H_2O_2 can be partly oxidized at the anode surface:

$$H_2O_2 \rightarrow HO_2^{\bullet} + H^+ + e^- \quad (3)$$

A second, fundamental feature of EF is the need of much lower concentrations of iron ions (down to two orders of magnitude), which results from the continuous cathodic Fe^{2+} regeneration that sustains the catalytic process:

$$Fe^{3+} + e^- \rightarrow Fe^{2+} \quad (4)$$

In a recent study, we investigated the PVP crosslinking activated by hydroxyl radicals electrogenerated through several approaches [44]. The interest of PVP as starting preformed polymer arises from its high versatility in biomedical applications. PVP shows high hydrophilicity and biocompatibility, absence of toxicity and ability to form interpolymer complexes [45]. It is used as plasma expander and additive in several pharmaceutical formulations. Emerging PVP-based materials include nanocarriers for gene therapy [46,47] or to enhance the delivery of biomolecules to the brain in the treatment of neurodegenerative diseases [8]. We provided the proof of concept that PVP crosslinking can be induced by an electrochemical process such as EF [44]. As a major feature, it is important to highlight that EF is a more accessible technology than radiation processing in terms of simplicity and safety, allowing an easy control of the various competing reactions upon accurate selection of experimental parameters.

The aim of this work is to carefully assess the role of key parameters that determine the electrochemically-induced transition from linear, water-soluble PVP to polymer nanogels by the formation of a crosslinked network under EF conditions. The effect of the electrolysis time, PVP and Fe^{2+} concentration, applied current and electric charge (Q) on the particle size and its polydispersity, molecular weight, functionalization and mineralization has been studied in detail using an undivided cell with an air-diffusion cathode and a dimensionally stable anode (DSA®). The extent of intra/intermolecular crosslinking depends on these factors, and their predominance is discussed along the paper. Note that, unlike usual work in other fields like environmental electrochemistry, where the highest production rate of •OH is preferred in order to have a very oxidizing environment, here it is critical to dose them adequately to prevent significant mineralization [48], and EF seems well-suited for this purpose.

2. Materials and methods

2.1. Chemicals

PVP k-60 (M_r = 1.60 × 10^5 g mol^{-1}, M_w = 3.95 × 10^5 g mol^{-1}, 45 wt.% solution) was purchased from Aldrich and used as received. PVP critical chain overlapping concentration in water (~1%) was determined by light scattering in a previous work [49]. Spectra/Por® cellullose acetate dialysis membranes of 12–14 kDa cutoff were purchased from Spectrum Laboratories, wheras 0.22 μm nylon and 1.22 μm cellulose acetate syringe filters were supplied by Aldrich. Oxygen (99.999% purity) and nitrogen (99.998% purity) were supplied by Air Liquide. Na_2SO_4 used as supporting electrolyte, H_2SO_4 added to work at pH 2.8, $FeSO_4$ employed as catalyst, KBr (FT-IR grade) needed for FT-IR analyses and NaN_3 for gel permeation chromatography (GPC) analyses were acquired from Sigma-Aldrich and Fluka. All solutions were prepared with double-distilled water.

2.2. Electrosynthesis system

For all the experiments, fresh PVP aqueous solutions were prepared and stirred overnight, filtered with 0.22 μm nylon filters under vacuum. An undivided glass cell equipped with a water jacket was used for the electrosynthesis of nanogels. An Ultratemp 2000 water bath from Julabo was employed to maintain the temperature of the solutions at 20 °C during the trials. In each run, the electrolytic cell contained 50 cm^3 of PVP solution at a given concentration with 0.05 M Na_2SO_4 in the presence of $FeSO_4$ as catalyst. The experiments were performed at pH 2.8, since this is the optimum value for Fenton's reaction (1) [42], under continuous stirring with a magnetic bar at 400 rpm to ensure fast mass transport of all reactants. A carbon-polytetrafluorethylene (PTFE) air-diffusion electrode from E-TEK was used as the cathode to electrogenerate H_2O_2 from reaction (2), whereas a Ti/IrO_2–Ta_2O_5 (DSA®) plate from ElectroCell AB, was used as anode. The geometric surface area of all electrodes in contact with PVP solution was 3 cm^2. The cathode was mounted as described elsewhere [42] and was fed with pressurized O_2 pumped at 0.5 dm^3 min^{-1} for H_2O_2 generation. An Amel 2053 potentiostat/galvanostat was employed to operate at constant current. All trials were carried out under galvanostatic conditions, which is preferable for controlling the rate of generation of hydroxyl radicals during the whole duration of the electrolyses when using a gas-diffusion electrode. In order to ascertain that the anode surface was completely clean and the cathode was activated prior to use, an electrolysis with both electrodes was carried out in 0.050 mol dm^{-3} Na_2SO_4 at 100 mA for 180 min. After each experiment, the final solution was filtered with 1.22 μm cellulose acetate syringe filters and stored for pursuing with all the analyses.

2.3. Analytical procedures

The H_2O_2 concentration accumulated from reaction (2) was determined from the absorbance of its colored complex with Ti(IV) at λ = 408 nm [50], using a Shimadzu 1800 UV/Vis spectrophotometer at 35 °C. For total organic carbon (TOC) analysis, samples were withdrawn from raw and treated solutions, filtered with 0.45 μm PTFE filters from Whatman and directly injected into a Shimadzu LCSH analyser. Reproducible values were obtained using the non-purgeable organic carbon mode. A 3:97 (v/v) methanol/water (0.1% acetic acid) mixture was eluted at 0.5 cm^3 min^{-1} as the mobile phase. Dynamic and multi-angle static light scattering (DLS and SLS) analysis for the evaluation of the hydrodynamic radius (R_h) and the weight-average molecular weight (M_w), respectively, were carried out using a Brookhaven BI-9000 correlator and a 50 mW He–Ne laser (Melles-Griot) tuned at λ = 532 nm, and the values were compared with those of the untreated linear PVP. In particular, DLS data were analyzed according to the method of cumulants [51], and the errors bars provided in the corresponding figures showing the R_h values account for the width of particle size distribution. The SLS data were analyzed according to the Zimm plott method using experimentally measured refractive index increments dn/dc values measured by using a Brookhaven Instruments differential refractometer at λ = 620 nm. Measurements were always carried out on replicate samples.

Gel Permeation Chromatography (GPC) analysis was performed with an Agilent 1100 Series HPLC equipped with two Shodex columns (804 and 806) in series, thermostated at 20 °C, and coupled to a refraction index (RI) detector at 35 °C. A solution of 3 mmol dm^{-3} NaN_3 was eluted at 0.5 cm^3 min^{-1} as mobile phase. FT-IR analyses for assessing the chemical changes undergone by PVP particles were recorded on a Perkin-Elmer Spectrum 400 and the samples were prepared after obtaining the solid nanoparticles by freeze drying. Weighed amounts of nanoparticles were mixed with KBr in a mortar and pressed into discs with a 10 ton pressure to obtain a film. The spectra were recorded at 32 scans per spectrum and 2 cm^{-1} resolution in the 4000–400 cm^{-1} range. After each electrosynthesis and prior to GPC and IR analysis, the salts (Na_2SO_4 and $FeSO_4$) were removed by dialysis in distilled water for 96 h employing cellulose acetate membranes (12 kDa cutoff).

3. Results and discussion

3.1. Oxidative environment under EF conditions

The ability of the air-diffusion cathode to electrogenerate H_2O_2 on site was first investigated through a series of electrolytic trials in 0.05 mol dm^{-3} Na_2SO_4 solutions at pH 2.8 and 20 °C under different conditions. As can be observed in Fig. 1, large accumulations of H_2O_2 can be achieved with this cathode in batch systems, as also reported in the case of flow cells with recirculation [50]. Therefore, this electrode material is expected to be optimum for performing H_2O_2-based electrochemical crosslinking, in contrast to less efficient carbonaceous cathodes [52]. In the absence of Fe^{2+} (i.e., electro-oxidation process) at 33.3 mA cm^{-2}, the H_2O_2 concentration showed a continuous increase with time, reaching 27.0 mmol dm^{-3} at 180 min. However, it must be noted that the efficiency was around 40% at 30 min, decaying at longer time as deduced from the non-linear profile of the curve. In undivided cells, this behavior may be associated with the competition between the H_2O_2 production at the cathode from reaction (2) and its destruction at the anode to yield $HO_2^{\bullet}$ from reaction (3), eventually tending to a H_2O_2 concentration plateau once both reaction rates equate (pseudo-steady state conditions). An analogous experiment made in the presence of 1.0 mmol dm^{-3} Fe^{2+} revealed a more pronounced non-linear behavior, attaining an almost steady H_2O_2 concentration of 11.0 mmol dm^{-3} at 180 min. This lower accumulation can then be related to the significant occurrence of Fenton's reaction (1), in concomitance with H_2O_2 disappearance by either reaction with Fe^{3+} or direct anodic oxidation. This result is an indication that the EF process is an effective source of $^{\bullet}OH$, and possibly also $HO_2^{\bullet}$, in the bulk solution. Fig. 1 also shows the influence of current density on the oxidative environment in EF systems. At 100 mA cm^{-2}, a slightly greater accumulation of H_2O_2 was obtained as a result of the faster O_2 reduction from reaction (2), ending in ca. 13 mmol dm^{-3} at 180 min. Nonetheless, the enhancement was not proportional to the current increase, which can be mainly explained by the quick H_2O_2 consumption upon reaction with (i) Fe^{2+}, speeding up the formation of $^{\bullet}OH$, and (ii) $^{\bullet}OH$ to yield $HO_2^{\bullet}$ as follows:

$$H_2O_2 + {}^{\bullet}OH \rightarrow HO_2^{\bullet} + H_2O \quad (5)$$

The presence of dissolved O_2 during the electrolyses has an impact on the outcome of the treatment. On the one hand, it affects the stability of C-centered polymer radicals ($R^{\bullet}$) [23], which are very quickly transformed into $ROO^{\bullet}$ first, to evolve into $RO^{\bullet}$ and stable oxygenated products, exhibiting carbonyl and alcohol groups [21]. But it also has influence on the production of reactive oxygen radicals that compete with OH under EF conditions. In the current setup, the main routes for O_2 dissolution in the aqueous matrices are: (i) the diffusion of excess of O_2 fed to the cathode, (ii) its evolution from water oxidation at the anode surface and (iii) its formation by chemi-

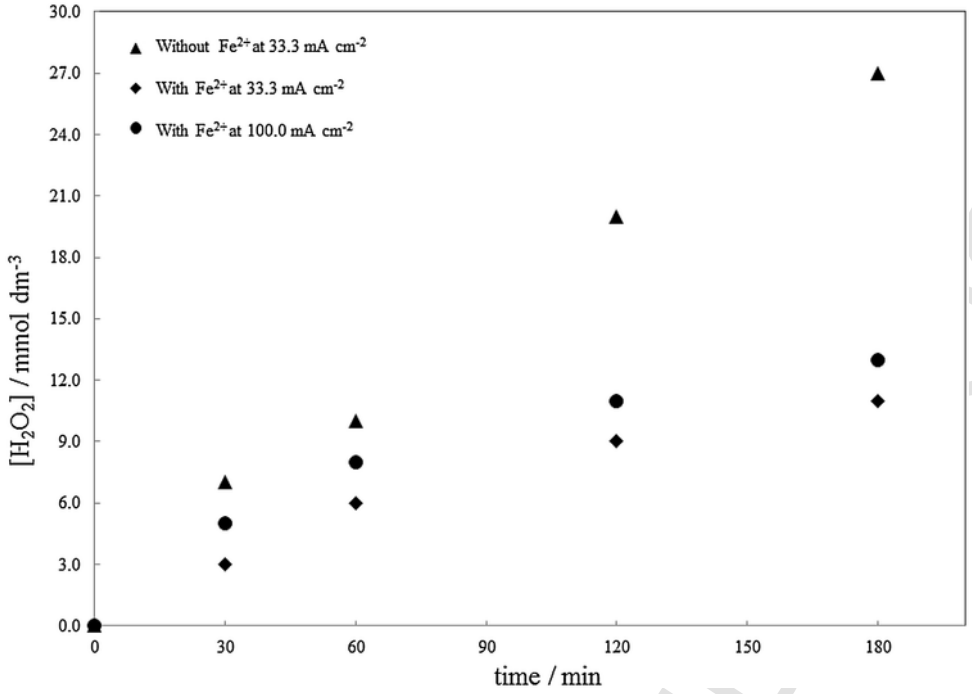

Fig. 1. Time course of the accumulated H_2O_2 concentration vs electrolysis time for the treatment of 50 cm^3 of 0.05 mol dm^{-3} Na_2SO_4 solutions at pH 2.8 and 20 °C using a cell with an air-diffusion cathode and an IrO_2-based anode, both of 3 cm^2 area, under different conditions.

cal decomposition of H_2O_2. Once dissolved, O_2 can lead to the formation of the superoxide radical, which is mainly transformed into its protonated form ($HO_2^{\bullet}$) at the reaction pH of 2.8 [34,42]:

$$Fe^{2+} + O_2 \rightarrow Fe^{3+} + O_2^{\bullet -} \quad (6)$$

Hydroxyl radicals, and possibly hydroperoxyl radicals, can react with preformed polymer chains leading to the formation of free radical centers on their backbone. These radical centers can be involved in termination reactions that can be intermolecular or intramolecular, whether the radicals are host by two different polymer chains or by the same chain, respectively. Termination occurs either by combination, which result in a crosslink point or by disproportionation that leads to simultaneous formation of one saturated and one unsaturated polymer chain segment. The activation energy for disproportionation is much higher than that for coupling and thus, for many polymers disproportionation takes places to a minor extent if compared to combination. It may become the predominant termination process if the macroradical is sterically hindered. If intermolecular combination is prevalent, the formation of polymer gel by crosslinking of different polymer chains can be observed. Conversely, intramolecular combination, that is made possible by conformational flexibility of the polymer chain, leads to the formation of an internally reticulated more compact coil without significant alteration of the molar mass of the macromolecule.

It must be considered that generated macroradicals can also evolve through β-scission thus leading to a reduction of the polymer molecular weight. The kinetic competition between crosslinking and chain scissioning of macroradicals essentially depends on the chemical structure of the polymer. Furthermore, also for polymers in which crosslinking prevails the relative rate of degradation with respect to crosslinking can significantly change if structural modifications of the polymer occur, such as an increase in rigidity due to crosslinking, or functionalization due to oxidation.

Considering a value of 63 (mol dm^{-3})$^{-1}$ s^{-1} for the kinetic constant of Fenton's reaction (1) [42], and Fe(II) and H_2O_2 concentrations of 10^{-3} and 10^{-2} mol dm^{-3}, respectively, which are the typical values that can be expected under operation conditions adopted in this study, the order of magnitude of the average rate of $^{\bullet}OH$ generation can be estimated to be $\sim 10^{-3}$ mol dm^{-3} s^{-1}. As discussed below, PVP solutions are prepared at 0.25-0.75 wt.%, which accounts for $\sim 10^{-4}$ mol dm^{-3} PVP. With such estimated values, an order of magnitude of 10 radicals s^{-1} per chain can be expected and hence, the formation of multiple radical centers on the polymer backbone is ensured. As demonstrated hereafter, the biasing between inter and intramolecular recombination of free radical centers can evolve with all parameters that affect the rate of generation of hydroxyl radicals and the molar concentration of polymer chains in the electrolytic solution.

3.2. Influence of various operation parameters on the formation of PVP nanogels by EF

In the presence of organic species like PVP, the $^{\bullet}OH$ along with the other reactive agents account for the modification of chains initiated by H abstraction from the polymer. Since semi-dilute PVP solutions are employed, the direct electron transfer to/from PVP chains can be disregarded. As a result, the main transformation routes are chain scission through successive cleavage, which promotes the decrease of the average molecular weight, or polymer crosslinking that leads to chain branching and 3D network formation. The relative competition between these pathways depends on the operation conditions, which also determine the extent of intra/intermolecular crosslinking. This information is crucial to optimize the reaction setup with the aim of obtaining a nanogel with specific properties in terms of particle size and density (R_h and M_w) as well as of chemical structure.

Fig. 2 shows the effect of electrolysis time on size of polymer coil (R_h) and on its M_w, measured by DLS and SLS, for the EF treatment

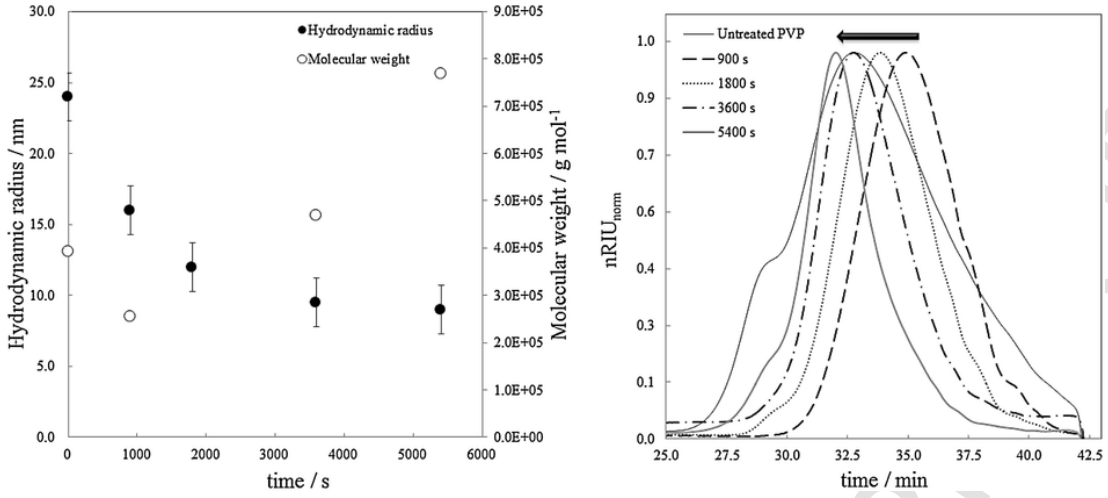

Fig. 2. (Left) Effect of electrolysis time on R_h and M_w for the EF treatment of 50 cm^3 of PVP at 0.25 wt.% with 0.05 mol dm^{-3} Na_2SO_4 in the presence of 1.0 mmol dm^{-3} $FeSO_4$ at pH 2.8, 33.3 mA cm^{-2} and 20 °C, using the same setup described in Fig. 1. (Right) GPC analyses of untreated and electrolyzed PVP samples obtained as described in the left panel.

of PVP at 0.25 wt.% with 0.05 mol dm^{-3} Na_2SO_4 in the presence of 1.0 mmol dm^{-3} $FeSO_4$ at pH 2.8, and 33.3 mA cm^{-2}, using the DSA®/air-diffusion cell described above. Furthermore, GPC analyses of the untreated and electrolyzed PVP samples are depicted in the right panel. Note that all the solutions were optically transparent upon electrolysis. TOC measurements suggested that no incineration of PVP chains occurred (not shown), in correspondence with the low charge passage (540C as maximum) as compared to that needed for total mineralization (ca. 4,000C, presupposing 100% of current efficiency).

When experiments of increasing duration (900 to 5,400 s) were made, a significant change of R_h and M_w was observed, thus confirming that the aforementioned oxidative environment in EF allows the formation of a large number of radical centers on dissolved polymer chains. More dilute PVP solutions (< 0.25 wt.%) did not show significant polymer modification when observed in the same time window, probably because the reaction of the hydroxyl radicals with the polymer were outcompeted by their mutual recombination and other wasting reactions [25,26]. The R_h showed a very remarkable decrease from 24 nm for the untreated PVP to 16, 12, 9 and 8 nm at 900, 1,800, 3,600 and 5,400 s, respectively, that was accompanied by an initial decrease of M_w from 3.95×10^5 g mol^{-1} to $2.5–3.0 \times 10^5$ g mol^{-1} for electrolyses up to 1,800 s, followed by a progressive increase of the weight average molecular weight up to 7.8×10^5 g mol^{-1} at 5,400 s. From the comparison among the GPC traces of electrolyzed polymer and that of the virgin PVP (Fig. 2, right panel) we can observe that after the initial 900 s the elution curve became narrower and mainly located at longer elution time, suggesting lower hydrodynamic volumes and hence, lower molecular weights. When the electrolysis time increased, the GPC traces moved to lower elution times, thus indicating that polymer chains with progressively higher hydrodynamic volume were formed, in good agreement with the increasing trend of average M_w from SLS measurements (note that no quantitative correlation can be established between the hydrodynamic volumes from GPC and hydrodynamic radii from DLS). The initial reduction of coil dimensions accompanied by M_w decrease can be explained by the reaction of carbon-center radicals with dissolved molecular oxygen forming oxygen-center radicals, which in turn can undergo unimolecular fragmentation. By increasing the electrolysis time, a further contraction of the particle size down to a plateau value, for 3,600 s of electrolysis and above was observed, now accompanied by a steep increase of molecular weight. This behavior could be attributed to the simultaneous occurrence of inter and intramolecular crosslinking. Indeed, the initial chain cleavage caused an increase of polymer molar concentration, which resulted in a higher scavenging capability of hydroxyl radicals by the polymer chains and in an increased probability of macroradicals termination by intermolecular combination. Linear polymer chains become branched and then crosslinked transforming into nanogels. The continuous generation of hydroxyl radicals produces radical sites also onto the slightly crosslinked nanogel embryos, which can mutually interpenetrate and crosslink; this causes a significant increase of M_w without a significant increase of particle size. Oxidative molecular degradation, that is always a competing process with crosslinking, can impact on the molecular weight of the nanogels much less than on that of the pristine linear chains; bond cleavage can involve chain segments between crosslinks that still remain attached to the network or dangling chains whose fragmentation does not affect very much the nanogel molecular weight. The GPC curves progressively shift towards the lower elution times, hence to the higher hydrodynamic volumes. Interestingly, the reduction in the polydispersity of the polymer, associated to narrower width of GPC curves (see right panel), is maintained throughout the process. This could be explained considering that in the starting highly polydisperse (i.e., multimodal) PVP, smaller chains mainly undergo intermolecular crosslinking while bigger chains are mainly involved in intramolecular combination. Indeed, the lower molecular weight fractions have a lower hydroxyl radical scavenging capacity and thus, form fewer radicals per chain. This favors their intermolecular combination over intramolecular one. Conversely, the higher molecular weight fractions can form more radicals per chain, condition that favors intramolecular crosslinking and polymer coil shrinkage.

In conclusion, the dimensions and density of the nanogel can be tuned up by controlling the electrolysis time. Worth noting, trials longer than 5,400 s did not lead to smaller polymer particles, which can be explained by the gradual loss of relative mobility of the chain segments upon coil shrinkage owing to covalent bond formation, impeding further intramolecular approach of radical centers.

The effect of PVP concentration within the range 0.25-0.75 wt.% on the time course of R_h for EF treatments analogous to those described in Fig. 2 is presented in Fig. 3. The maximum PVP content was 0.75 wt.% because higher values cause significant chain overlapping and broadening of particle size distribution. [49]. As can be ob-

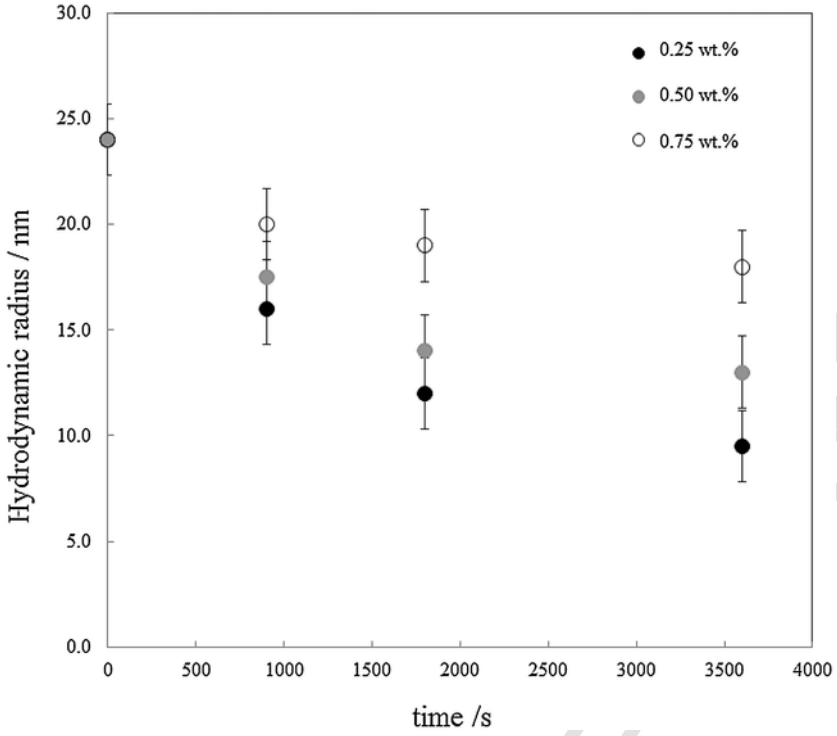

Fig. 3. Effect of PVP concentration on the time course of R_h for EF treatments as described in Fig. 2.

served, the time course of R_h shows a similar profile at all PVP concentrations, with a continuous decrease as the electrolysis time increased. However, the decay from the initial value of 24 nm was less pronounced at higher PVP content, with R_h values of 17.5, 14 and 13 nm at 0.50 wt.% and 20, 19 and 18 nm at 0.75 wt.% for EF treatments prolonged for 900, 1,800 and 3,600 s, respectively. This behavior could be attributed to a decrease of the average number of radicals per chain that are generated at fixed rate of production of hydroxyl radicals as a consequence of the higher concentration of polymer chains. As expected, the polymer concentration is one other important tunable parameter to control the particle size, by changing the relative weight of the different competing reactions that govern the yield of macroradicals and their follow up reactions.

One major advantage of EF compared to non-electrochemical Fenton processes is the low amount of Fe^{2+} ions typically needed for maintaining the catalytic cycle for long periods [42]. Fig. 4 (left panel) shows the effect of catalyst concentration on R_h and M_w for the EF treatment of PVP solutions at 0.25 wt.% with 0.05 mol dm^{-3} Na_2SO_4 at pH 2.8 and 33.3 mA cm^{-2} for 3,600 s. The corresponding GPC analyses of untreated and electrolyzed samples are presented in the right panel. The use of a very small amount like 0.1 mmol dm^{-3} Fe^{2+} allowed the reduction of R_h from 24 to 16 nm, which confirms the ability of this technology to generate •OH via reaction (1) and achieve a significant modification of raw PVP. However, under the same conditions, M_w decreased to ca. 1.0×10^5 g mol^{-1}. From these results, it can be said that such a small Fe^{2+} concentration is not opti-

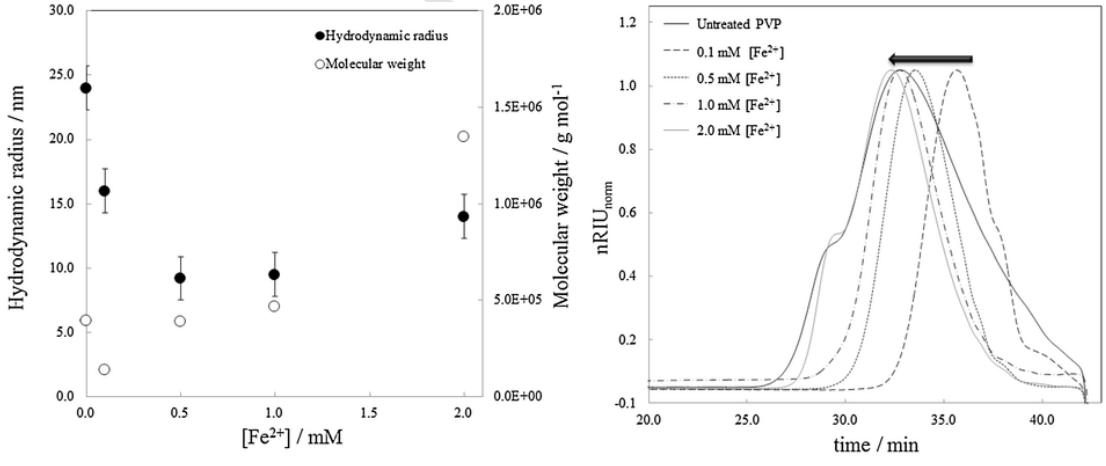

Fig. 4. (Left) Effect of catalyst (Fe^{2+}) concentration on R_h and M_w for the EF treatment of 50 cm^3 of PVP at 0.25 wt.% with 0.05 mol dm^{-3} Na_2SO_4 at pH 2.8, 33.3 mA cm^{-2} and 20 °C for 3600 s, using the same setup described in Fig. 1. (Right) GPC analyses of untreated and electrolyzed PVP samples obtained as described in the left panel.

mal since it basically promotes a considerable extent of chain cleavage that is not adequately counterbalanced by crosslinking, owing to the very low rate of macroradicals formation and low probability of their mutual combination in the oxygen saturated solution. A different performance was found when the transition metal ion concentration was increased to low-intermediate values (0.5-1.0 mmol dm^{-3}). Within this range, the R_h decreased to 8.5–9 nm, whereas the M_w was kept almost constant at 0.5 mmol dm^{-3} Fe^{2+}, and slightly increased to 4.8×10^5 g mol^{-1} at 1.0 mmol dm^{-3}. The greater presence of Fe^{2+} ions accounted for a higher rate of production of active •OH, therefore for the higher momentary concentration of macroradicals that make their inter/intramolecular crosslinking more competitive. Finally, the highest Fe^{2+} content in the explored range (2.0 mmol dm^{-3}) favored even more both inter- and intramolecular crosslinking, resulting in nanogels with 4-fold increase of M_w and a ca. half R_h with respect to corresponding values for the untreated polymer. An increase of Fe^{2+} did not favor crosslinking any further (data not shown), probably due to the faster hydroxyl radical consumption as follows [42]:

$$Fe^{2+} + {}^{\bullet}OH \rightarrow Fe^{3+} + OH^{-} \quad (7)$$

The right panel in Fig. 4 suggests an evident reduction of polydispersity for EF trials carried out in all the investigated conditions.

The effect of catalyst concentration on the chemical structure of polymer nanogels was also qualitatively assessed by IR analysis, as shown in Fig. 5. It can be seen that the EF treatment induced qualitatively the same chemical modifications on PVP, irrespective of the Fe^{2+} concentration present in the system. In particular, higher absorptions were observed in the 3,700-3,000 cm^{-1} region, which can be related to: (i) the stretching of hydroxyl group, which is present from either adsorbed water or polymeric hydroxyl groups [27,53], and (ii) N-H stretching vibrations [28]. The tail from that band overlaps with the —CH_2 band (at 2,500 cm^{-1}) as a result of hydroxyl-to-carbonyl coupling of —COOH groups. The presence of carbonyl/carboxylate groups is supported by the absorption at 1,400 cm^{-1} (signal *c* in the inset panel) [26]. In addition, EF caused the increase of absorption at 1,661 cm^{-1} present in the untreated PVP, which is related to carbonyl stretching of the pyrrolidone ring, along with the formation of a couple of new peaks at 1,695 and 1,765 cm^{-1} (signals *b* and *a*, respectively). They could probably be associated to symmetric/asymmetric stretching of a cyclic imide (i.e., succinimide) formed upon hydroxylation of the carbon atom next to the nitrogenated carbon of the ring [44]. A band appearing at 820 cm^{-1}, related to the twisting of —CH_2, reinforces the hypothesis of succinimide formation. Furthermore, the presence of the two carbonyl groups of succinimide favors the formation of —COOH from oxidative scission caused by •OH attack on those carbon atoms. The action of H_2O_2 and O_2 may contribute to such scissions [28]. Worth mentioning, the greatest absorptions for all peaks described above were obtained with the lowest Fe^{2+} concentration (0.1 mmol dm^{-3}). Probably, the lower production rate of carbon-center radicals and larger accumulation of H_2O_2 at lower Fe^{2+} concentration (see also Fig. 1) both contribute to the more evident appearance of all those new functionalities.

3.3. Influence of total amount of •OH produced and •OH production rate

In radiolysis-based crosslinking, both the absorbed radiation dose and the dose-rate are critical parameters because they determine the

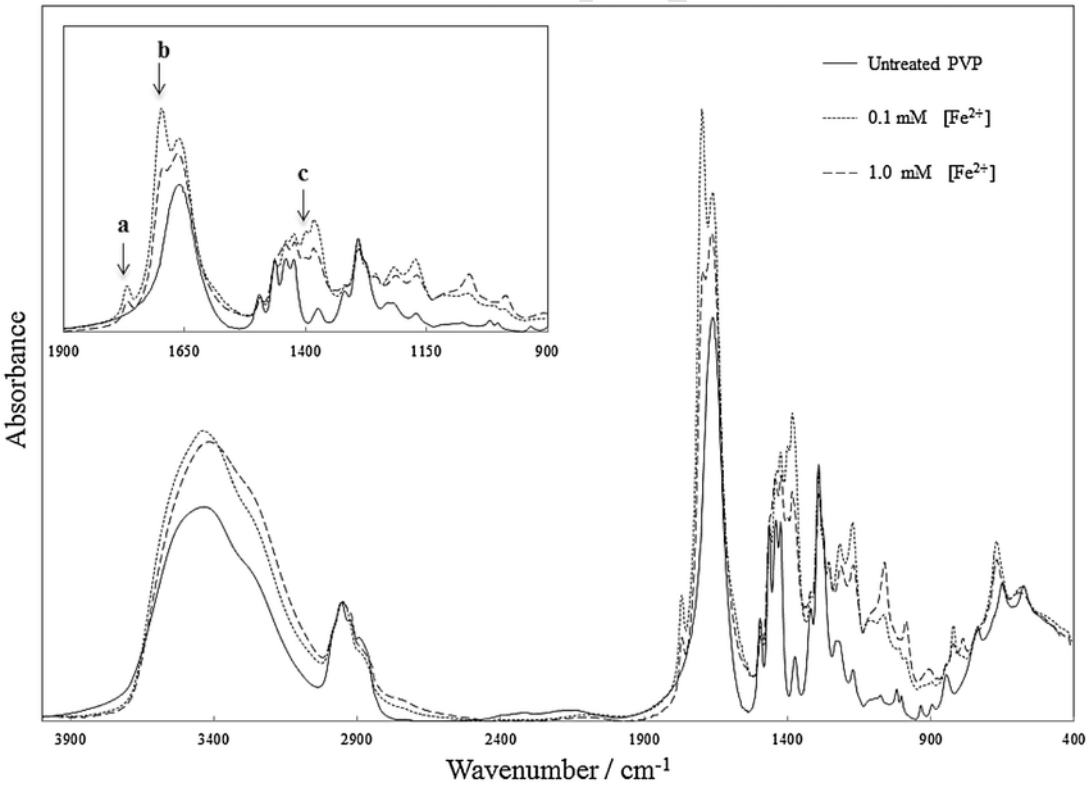

Fig. 5. FT-IR spectra of PVP samples at 0.25 wt.%, both untreated and electrolyzed by EF as described in Fig. 4. In the inset panel, enlargement of the region between 1900 and 900 cm^{-1}, where the arrows indicate peaks that appear upon electrolysis.

total amount of •OH produced and their momentary concentration, respectively. The first parameter affects the extent of molecular and/or chemical modification induced on the irradiated polymer, whereas the latter governs the kinetics of the various competing processes. To test the effect of the total amount of •OH generated and their production rate in the current EF system, various electrolyses were made at different j values, since this is the parameter that controls the production rate of H_2O_2 from reaction (2) and thus, it is another parameter affecting the rate of •OH generation from Fenton's reaction (1). First, EF trials were carried out at 33.3, 100.0 and 166.7 mA cm^{-2} for a fixed time of 10,800 s, which corresponds to increasing electric charges (i.e., •OH doses) as shown in Fig. 6, using PVP at 0.50 wt.% and 1.0 mmol dm^{-3} $FeSO_4$. In all cases, the chromatographic peak of treated PVPs was eluted at longer time compared to that of the untreated polymer, suggesting the formation of smaller PVP nanoparticles with lower polydispersity. The R_h and M_w values summarized in Table 1 (entries 1–3) indicate a clear size reduction up to about 10–11 nm, as well as an average two-fold decrease of M_w at all adopted current density The trend of R_h agrees with that reported in Fig. 3, indicating that it is not feasible to reduce the size below 10 nm working with PVP solutions > 0.25 wt.%. Conversely, according to Fig. 2, a long EF treatment between 1,800 and 5,400 s conducted at 0.25 wt.% at a low j of 33.3 mA cm^{-2} led to a significant increase of M_w resulting from an enhanced intermolecular crosslinking, whereas Fig. 6 reveals that excessively long EF trials, even at low j, yield M_w values that are lower than the initial one. This unexpected decay can be explained considering that, in prolonged experiments, a 3D nanogel network that has grown considerably via intermolecular crosslinking can guest many radical centers per macromolecules. However the high rigidity imposed to these molecular species by internal crosslinks prevents further intramolecular decay of these radical centers, thereby promoting chain scission. The same was found as j increased, with cleavage prevailing at such long electrolysis time. Obviously, at high j, a large fraction of •OH was lost through radical-

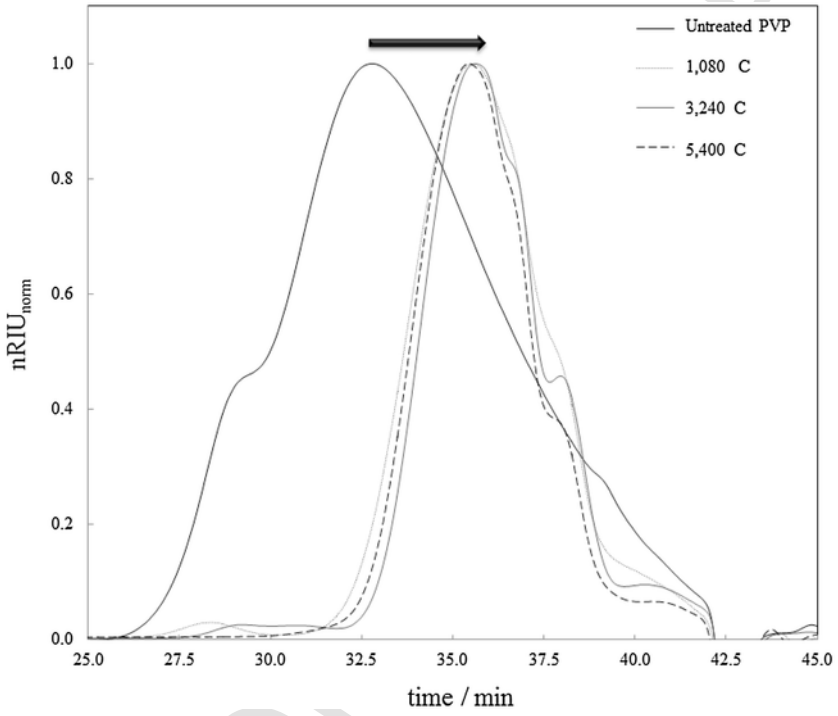

Fig. 6. Effect of electric charge passed for 10,800 s on the molecular weight distribution obtained by GPC analysis for the EF treatment of 50 cm^3 of PVP at 0.50 wt.% with 0.05 mol dm^{-3} Na_2SO_4 in the presence of 1.0 mmol dm^{-3} $FeSO_4$ at pH 2.8 and 20 °C, using the same setup described in Fig. 1. Current density as charge increases: 33.3, 100.0 and 166.7 mA cm^{-2}.

Table 1
Results obtained for the modification of PVP at different current densities and electric charges. All experiments were performed with 0.50 wt.% PVP in 0.05 mol dm^{-3} Na_2SO_4 with 1.0 mmol dm^{-3} Fe_2SO_4, at pH 2.8 and 20 °C.

Entry	j (mA cm^{-2})	t (s) − Q (C)	Q/Q_{th}			R_h (nm)	TOC decay (%)	$M_w \times 10^{-5}$(g mol^{-1})
			Mineralization[a]	1-H per monomeric unit[b]	1 H per chain[c]			
PVP-k60						24.0 ± 6.1		3.95 ± 0.15
1	33.3	10,800–1,080	0.146	5.0	7,160	11.2 ± 3.2	1	2.2 ± 0.20
2	100.0	10,800–3,240	0.439	14.9	21,500	10.9 ± 3.5	<1	1.7 ± 0.16
3	166.7	10,800–5,400	0.731	24.8	35,800	10.8 ± 2.7	<1	2.5 ± 0.20
4	166.7	2,160–1,080	0.146	5.0	7,160	12.7 ± 3.5	<1	2.3 ± 0.19

[a] Theoretical charge (Q_{th}) is that needed for the complete mineralization of PVP.

[b] Q_{th} refers to the abstraction of 1 H atom per each monomeric unit.

[c] Q_{th} refers to the abstraction of 1 H atom per each polymer chain.

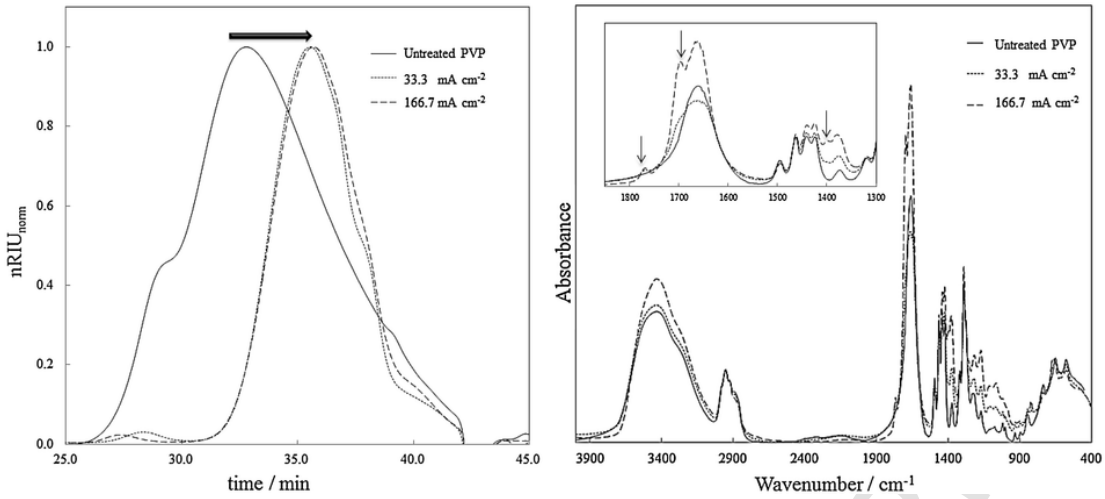

Fig. 7. (Left) Effect of current density at a fixed electric charge of 1,080C on the molecular weight distribution obtained by GPC analysis for EF treatments as described in Fig. 6. (Right) FT-IR spectra corresponding to the same trials.

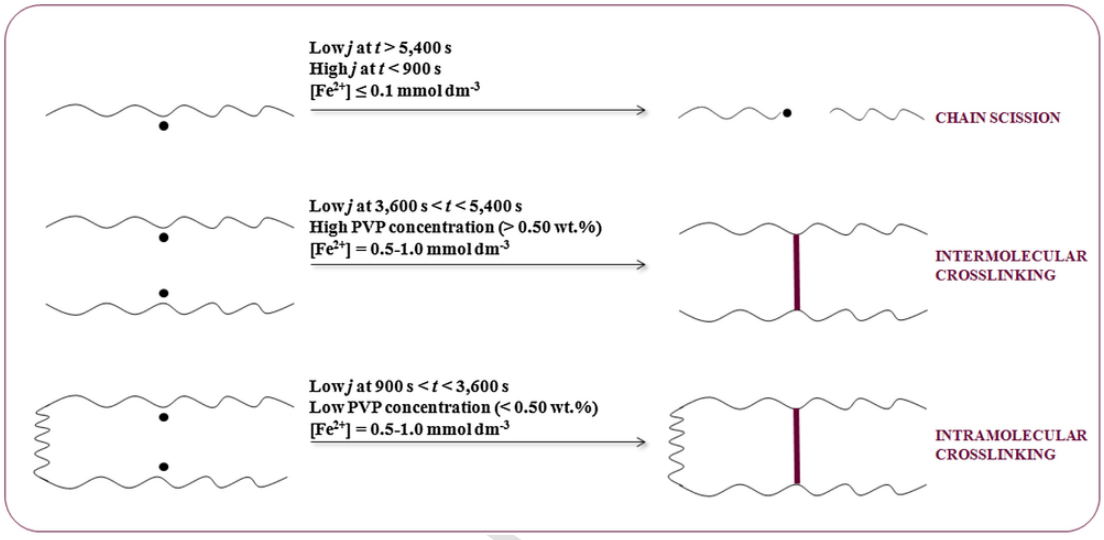

Fig. 8. Correlation of all the studied operation conditions with the prevailing mechanism (chain scission, intermolecular and intramolecular crosslinking) of PVP modification under EF conditions.

radical combination reactions, ending in H_2O_2, which explains the similar results obtained for the three *j* values tested.

To demonstrate that polymer modification is not a matter of the electrolysis time or the current density value alone, Fig. 7 compares the effect of two *t*-*j* sets at a fixed *Q* of 1,080C. As can be seen in the left panel, the same elution peaks were obtained by GPC at either long *t*/low *j* or short *t*/high *j*. Furthermore, similar R_h and M_w values were obtained for the two experiments as summarized in Table 1 (entries 1 and 4). However, despite the fact that the EF treatment at a fixed *Q* yielded PVP nanoparticles of same size and mass, the specific value of *j* had an impact on the degree of functionalization (i.e., formation of succinimide and —COOH groups as discussed from Fig. 5) of the chains. As depicted in the right panel of Fig. 7, peaks from FT-IR analysis displayed a higher intensity at a greater *j* of 166.7 mA cm^{-2}, which may be associated with a stronger oxidative transformation of PVP resulting from a quicker H_2O_2 (and thus, •OH) generation. When many of the macroradicals simultaneously formed cannot undergo mutual recombination because they are too isolated or the chains are too rigid, they evolve in oxidized groups.

To summarize all the aforementioned effects of operation parameters on the prevailing mechanism (chain scission, intermolecular and intramolecular crosslinking) of PVP modification under EF conditions, a scheme is shown in Fig. 8. Finally, it is worth mentioning that PVP crosslinking via EAOPs is plausibly accompanied by the simultaneous sterilization of the synthesized nanogel, as demonstrated from the electrochemical inactivation of various microorganisms [54], which is a positive collateral effect for biomedical applications of these materials.

4. Conclusions

PVP crosslinking by EF is feasible and opens the door to a cheap, eco-friendly, simple and fast alternative to current technologies. The adoption of different operation conditions is crucial for tuning up the characteristics of the resulting PVP nanogel in terms of particle size,

mass and functionalization, which are modulated by the rate of generation of •OH obtained from in situ electrogenerated H_2O_2. This affects the rate of formation of polymer radicals by H-abstraction, and the competition between their mutual combination reactions as well as the reaction with molecular oxygen that is mainly introduced by anodic oxidation of water. In general terms, smaller size and smaller molecular mass of polymer nanoparticles are obtained by EF starting from solutions at the same polymer concentration subjected to e-beam irradiation, as reported elsewhere. Semi-dilute (< 0.50 wt.%) PVP solutions are required to diminish the probability of intermolecular events in order to control the size of nanogel particles by inter/intra-molecular crosslinking. A low j of 33.3 mA cm^{-2} and relatively short electrolysis times (<3,600 s) are needed in case that a significant increase of M_w from intermolecular crosslinking is not aimed, whereas an excessive •OH dose resulting from high Q values (i.e., prolonged electrolysis and/or too high j) promotes chain scission that ends in low M_w values. The optimum range for catalyst concentration is 0.5–1.0 mmol dm^{-3}, since lower and higher Fe^{2+} contents induce chain scission and excessive intermolecular crosslinking, respectively. In all cases, a reduction in polydispersity was achieved. Interestingly, the action of •OH leads to the appearance of specific functionalities like —COOH and imide that can confer important properties and favor further (bio)conjugation. In conclusion, biocompatible and functionalized PVP nanocarriers can be obtained by EF treatment, with a potential market related to emerging biomedical applications.

Acknowledgement

The authors thank Università di Palermo for support under project FR 2012/13 ID 2014-ATE-0054.

References

[1] J.K. Oh, R. Drumright, D.J. Siegwart, K. Matyjaszewski, The development of microgels/nanogels for drug delivery applications, Prog. Polym. Sci. 33 (2008) 448–477.
[2] A.V. Kabanov, S.V. Vinogradov, Nanogels as pharmaceutical carriers: Finite networks of infinite capabilities, Angew. Chem. Int. Ed. 48 (2009) 5418–5429.
[3] S.V. Vinogradov, T.K. Bronich, A.V. Kabanov, Nanosized cationic hydrogels for drug delivery: preparation, properties and interactions with cells, Adv. Drug Delivery Rev. 54 (2002) 135–147.
[4] J. Ramos, J. Forcada, R. Hidalgo-Alvarez, Cationic polymer nanoparticles and nanogels: From synthesis to biotechnological applications, Chem. Rev. 114 (2014) 367–428.
[5] M. Elsabahy, G.S. Heo, S.-M. Lim, G. Sun, K.L. Wooley, Polymeric nanostructures for imaging and therapy, Chem. Rev. 115 (2015) 10967–11011.
[6] J.-Z. Du, T.-M. Sun, W.-J. Song, J. Wu, J. Wang, Tumor-acidity-activated charge-conversional nanogel as an intelligent vehicle for promoted tumoral-cell uptake and drug delivery, Angew. Chem. Int. Ed. 49 (2010) 3621–3626.
[7] C. Dispenza, G. Adamo, M.A. Sabatino, N. Grimaldi, D. Bulone, M.L. Bondì, S. Rigogliuso, G. Ghersi, Oligonucleotides-decorated-poly(N-vinyl pyrrolidone) nanogels for gene delivery, J. Appl. Polym. Sci. 131 (2014) 39974.
[8] K. Nagahama, Y. Sano, T. Kumano, Anticancer drug-based multifunctional nanogels through self-assembly of dextran–curcumin conjugates toward cancer theranostics, Bioorg. Med. Chem. Lett. 25 (2015) 2519–2522.
[9] G. Adamo, N. Grimaldi, S. Campora, D. Bulone, M.L. Bondì, M. Al-Sheikhly, M.A. Sabatino, C. Dispenza, G. Ghersi, Multi-functional nanogels for tumor targeting and redox-sensitive drug and siRNA delivery, Molecules 21 (2016) 1594.
[10] P. Picone, L.A. Ditta, M.A. Sabatino, V. Militello, P.L. San Biagio, M.L. Di Giacinto, L. Cristaldi, D. Nuzzo, C. Dispenza, D. Giacomazza, M. Di Carlo, Ionizing radiation-engineered nanogels as insulin nanocarriers for the development of a new strategy for the treatment of Alzheimer's disease, Biomaterials 80 (2016) 179–194.
[11] S. Yu, J. Hu, X. Pan, P. Yao, M. Jiang, Stable and pH-sensitive nanogels prepared by self-assembly of chitosan and ovalbumin, Langmuir 22 (2006) 2754–2759.
[12] G.C. Le Goff, R.L. Srinivas, W.A. Hill, P.S. Doyle, Hydrogel microparticles for biosensing, Europ. Polym. J. 72 (2015) 386–412.
[13] W. Wu, S. Zhou, Hybrid micro-/nanogels for optical sensing and intracellular imaging, Nano Rev. 1 (2010) 5730.
[14] M.A. Akl, A.A. Sarhan, K.R. Shoueir, A.M. Atta, Application of crosslinked ionic poly(vinyl alcohol)nanogel as adsorbents for water treatment, J. Dispers. Sci. Technol. 34 (2013) 1399–1408.
[15] M. Resmini, K. Flavin, D. Carboni, Microgels and nanogels with catalytic activity, Top Curr. Chem. 325 (2012) 307–342.
[16] V. Sáez-Martínez, B. Olalde, M.J. Juan, M.J. Jurado, N. Garagorri, I. Obieta, Novel bioactive scaffolds incorporating nanogels as potential drug eluting devices, J. Nanosci. Nanotechnol. 10 (2010) 2826–2832.
[17] G. Tillet, B. Boutevin, B. Ameduri, Chemical reactions of polymer crosslinking and post-crosslinking at room and medium temperature, Prog. Polym. Sci. 36 (2011) 191–217.
[18] K.S. Soni, S.S. Desale, T.K. Bronich, Nanogels: An overview of properties, biomedical applications and obstacles to clinical translation, J. Control. Release 240 (2016) 109–126.
[19] C. Dispenza, G. Spadaro, M. Jonsson, Radiation engineering of multifunctional nanogels, Top Curr. Chem. (Z) 374 (2016) 69.
[20] Y. Jiang, J. Chen, C. Deng, E.J. Suuronen, Z. Zhon, Click hydrogels, microgels and nanogels: Emerging platforms for drug delivery and tissue engineering, Biomaterials 35 (2014) 4969–4985.
[21] J.W.T. Spinks, R.J. Woods, An Introduction to Radiation Chemistry, Edited by Wiley-Interscience, John Wiley and Sons, New York, NY, USA, 1990.
[22] P. Ulański, I. Janik, J.M. Rosiak, Radiation formation of polymeric nanogels, Radiat. Phys. Chem. 52 (1998) 289–294.
[23] C. Dispenza, N. Grimaldi, M.A. Sabatino, I.L. Soroka, M. Jonsson, Radiation-engineered functional nanoparticles in aqueous systems, J. Nanosci. Nanotechnol. 15 (5) (2015) 3445–3467.
[24] J.-C. An, A. Weaver, B. Kim, A. Barkatt, D. Poster, W.N. Vreeland, J. Silverman, M. Al-Sheikhly, Radiation-induced synthesis of poly(vinylpyrrolidone) nanogel, Polymer 52 (2011) 5746–5755.
[25] M.A. Sabatino, D. Bulone, M. Veres, A. Spinella, G. Spadaro, C. Dispenza, Structure of e-beam sculptured poly(N-vinylpyrrolidone) networks across different length-scales, from macro to nano, Polymer 54 (1) (2013) 54–64.
[26] C. Dispenza, M.A. Sabatino, N. Grimaldi, M.R. Mangione, M. Walo, E. Murugan, M. Jonsson, On the origin of functionalization in one-pot radiation synthesis of nanogels from aqueous polymer solutions, RSC Adv. 6 (2016) 2582–2591.
[27] C. Dispenza, M.A. Sabatino, N. Grimaldi, D. Bulone, M.L. Bondì, M.P. Casaletto, S. Rigogliuso, G. Adamo, G. Ghersi, Minimalism in radiation synthesis of biomedical functional nanogels, Biomacromolecules 13 (2012) 1805–1817.
[28] N. Grimaldi, M.A. Sabatino, G. Przybytniak, I. Kaluska, M.L. Bondi, D. Bulone, S. Alessi, G. Spadaro, C. Dispenza, High-energy radiation processing, a smart approach to obtain PVP-graft-AA nanogels, Radiat. Phys. Chem 94 (1) (2014) 76–79.
[29] R.A. Wach, B. Rokita, N. Bartoszek, Y. Katsumura, P. Ulanski, J.M. Rosiak, Hydroxyl radical-induced crosslinking and radiation-initiated hydrogel formation in dilute aqueous solutions of carboxymethylcellulose, Carbohydrate Polym. 112 (2014) 412–415.
[30] L.C. Lopérgolo, A.B. Lugão, L.H. Catalani, Direct UV photocrosslinking of poly(N-vinyl-2-pyrrolidone) (PVP) to produce hydrogels, Polymer 44 (2003) 6217–6222.
[31] G.J.M. Fechine, J.A.G. Barros, L.H. Catalani, Poly(N-vinyl-2-pyrrolidone) hydrogel production by ultraviolet radiation: new methodologies to accelerate crosslinking, Polymer 45 (2004) 4705–4709.
[32] V.B. Bueno, I.M. Cuccovia, H. Chaimovich, L.H. Catalani, PVP superabsorbent nanogels, Coll. Polym. Sci. 287 (2009) 705–713.
[33] D. Xu, J. Hong, K. Sheng, L. Dong, S. Yao, Preparation of polyethyleneimine nanogels via photo-Fenton reaction, Rad. Phys. Chem. 76 (2007) 1606–1611.
[34] J.J. Pignatello, E. Oliveros, A. MacKay, Advanced oxidation processes for organic contaminant destruction based on the Fenton reaction and related chemistry, Crit. Rev. Environ. Sci. Technol. 36 (2006) 1–84.
[35] M.A. Oturan, J.J. Aaron, Advanced oxidation processes in water/wastewater treatment: Principles and applications. A review, Crit. Rev. Environ. Sci. Technol 44 (2014) 2577–2641.
[36] O.B. Ayodele, Structure and reactivity of ZSM-5 supported oxalate ligand functionalized nano-Fe catalyst for low temperature direct methane conversion to methanol, Energy Conv. Manage. 126 (2016) 537–547.
[37] K. Oueslati, D. de La Pomélie, V. Santé-Lhoutellier, P. Gatellier, Impact of the Fenton process in meat digestion as assessed using an in vitro gastro-intestinal model, Food Chem 209 (2016) 43–49.
[38] C. Saporito-Magriñá, R. Musacco-Sebio, J.M. Acosta, S. Bajicoff, P. Paredes-Fleitas, A. Boveris, M.G. Repetto, Rat liver mitocondrial dysfunction by addition of copper(II) or iron (III) ions, J. Inorg. Biochem. 166 (2017) 5–11.

[39] W.-P. Li, C.-H. Su, Y.-C. Chang, Y.-J. Lin, C.-S. Yeh, Ultrasound-induced reactive oxygen species mediated therapy and imaging using a Fenton reaction activable polymersome, ACS Nano 10 (2016) 2017–2027.
[40] Q. Xu, Y. Liu, R. Su, L. Cai, B. Li, Y. Zhang, L. Zhang, Y. Wang, Y. Wang, N. Li, X. Gong, Z. Gu, Y. Chen, Y. Tan, C. Dong, T.S. Sreeprasad, Highly fluorescent Zn-doped carbon dots as Fenton reaction-based bio-sensors: an integrative experimental–theoretical consideration, Nanoscale 8 (2016) 17919–17927.
[41] G. Feng, P. Cheng, W. Yan, M. Boronat, X. Li, J.-H. Su, J. Wang, Y. Li, A. Corma, R. Xu, J. Yu, Accelerated crystallization of zeolites via hydroxyl free radicals, Science 351 (2016) 1188–1191.
[42] E. Brillas, I. Sirés, M.A. Oturan, Electro-Fenton process and related electrochemical technologies based on Fenton's reaction chemistry, Chem. Rev. 109 (2009) 6570–6631.
[43] C.A. Martínez-Huitle, M.A. Rodrigo, I. Sirés, O. Scialdone, Single and coupled electrochemical processes and reactors for the abatement of organic water pollutants: A critical review, Chem. Rev. 115 (2015) 13362–13407.
[44] A. Galia, S. Lanzalaco, M.A. Sabatino, C. Dispenza, O. Scialdone, I. Sirés, Crosslinking of poly(vinylpyrrolidone) activated by electrogenerated hydroxyl radicals: A first step towards a simple and cheap synthetic route of nanogel vectors, Electrochem. Commun. 62 (2016) 64–68.
[45] M. Teodorescu, M. Bercea, Poly(vinylpyrrolidone) −A versatile polymer for biomedical and beyond medical applications, Polym. Plast. Technol. Eng. 54 (2015) 923–943.
[46] L. Zhang, Y. Liang, L. Meng, C. Wang, Characterization of complexation of PVP copolymer with DNA, Polym. Adv. Technol. 20 (2009) 410–415.
[47] Y. Song, T. Zhang, X. Song, L. Zhang, C. Zhang, J. Xing, X.-J. Liang, Polycations with excellent gene transfection ability based on PVP-g-PDMAEMA with random coil and micelle structures as non-viral gene vectors, J. Mater. Chem. B 3 (2015) 911–918.
[48] S. Ghafoori, M. Mehrvar, P.K. Chan, A statistical experimental design approach for photochemical degradation of aqueous polyacrylic acid using photo-Fenton-like process, Polym. Degrad. Stab. 110 (2014) 492–497.
[49] C. Dispenza, M. Ricca, C. LoPresti, G. Battaglia, M. La Valle, D. Giacomazza, D. Bulone, E-beam irradation and UV photocrosslinking of microemulsion-laden poly(N-vinyl-2-pyrrolidone) hydrogels for in-situ encapsulation of volatile hydrophobic compounds, Polym. Chem. 2 (2011) 192–202.
[50] G. Coria, I. Sirés, E. Brillas, J.L. Nava, Influence of the anode material on the degradation of naproxen by Fenton-based electrochemical processes, Chem. Eng. J. 304 (2016) 817–825.
[51] D.E. Koppel, Analysis of macromolecular polydispersity in intensity correlation spectroscopy: the method of cumulants, J. Chem. Phys. 57 (1972) 4814–4820.
[52] I. Sirés, J.A. Garrido, R.M. Rodríguez, E. Brillas, N. Oturan, M.A. Oturan, Catalytic behavior of the Fe^{3+}/Fe^{2+} system in the electro-Fenton degradation of the antimicrobial chlorophene, Appl. Catal. B: Environ. 72 (2007) 382–394.
[53] X. Zhu, P. Lu, W. Chen, J. Dong, Studies of UV crosslinked poly(N-vinylpyrrolidone) hydrogels by FTIR, Raman and solid-state NMR spectroscopies, Polymer 51 (2010) 3054–3063.
[54] C. Bruguera-Casamada, I. Sirés, M.J. Prieto, E. Brillas, R.M. Araujo, The ability of electrochemical oxidation with a BDD anode to inactivate Gram-negative and Gram-positive bacteria in low conductivity medium, Chemosphere 163 (2016) 516–524.